Theoretical investigation of charged vacancies and clusters in UXO2(X=La, Ce, Pu, Am)

Johann Bouchet, Rivo Diannzinga, Gerald Jomard

Theoretical investigation of charged vacancies and clusters in UXO_2 (X=La, Ce, Pu, Am)

J. Bouchet and R. M. Dianzinga and G. Jomard
CEA, DES, IRESNE, DEC, SESC, LM2C, F-13108 Saint-Paul-Lez-Durance, France

We present our ab-initio study of UXO_2 (X=La, Ce, Pu, Am) compounds. Depending of the ionization of the associated element, trivalent or tetravalent, either uranium stays tetravalent as in UO_2 either it is pentavalent to compensate the charge. We study the evolution of the lattice parameter as a function of X centent and in the presence of oxygen vacancies. We also calculate the formation energies of several vacancy defects and show that depending of the ionic state of X the most stable charge state can be either positive (tetravalent: Ce, Pu) or negative (trivalent: La, Am). We also consider the positron lifetime in the presence of these vacancies and we show that it is almost independent of the doping element and its amount. For uranium vacancies the positron is always trapped while for oxygen vacancies the trapping seems to depend of the surrounding cation oxidation states. Finally we show that different defects have similar positron lifetimes, resulting in extremely difficult defect identification with dedicated experimental studies as the positron annihilation spectroscopy.

I. INTRODUCTION

Uranium dioxide and (U, Pu)O2 mixed oxide with a Pu content of around 10% are the most widely used fuel material in fission reactors. During its burn-up, ^{235}U fission causes introduces fission products (FP) leading to chemical evolution and to a new complex material containing up to about 10 % of plutonium and minor actinides and 10-30 % of FP depending on the initial composition of the fuel and its burning time. At the same time, the fission of actinide nuclei causes the creation of large amounts of defects (vacancies, interstitial oxygens, bubbles, and dislocation loops), which could create local non-stoichiometric domains in the matrix. Understand the interplay between the FPs and the generated defects is one of the most important challenge in nuclear industry for the reactors performance and safety but also for the long term storage of spent fuels.

Among the elements produced either by fission or neutron capture, some are isovalent with uranium (as Pu or Ce) while others are aliovalent (as most of the lanthanides or some actinides like Am). The substitution of U by another cation of lower valence induces a deficit of charge that can be compensate either by a valence increase of uranium atom to U^{V+} or the formation of oxygen vacancy. The first mechanism was recently assessed as the major one in stoichiometric $U_{1-y}La_yO_2$[1] using complementary experimental techniques, with the conclusion that U^{V+} is formed in quasi-equimolar proportion as La^{III+} and the fluorite structure is maintained despite the cationic substitution. But the variations of the oxygen content, often designated as the oxygen-to-metal (O/M) ratio could restore the neutral charge for other element. From a structural point of view, these (O/M) variations can lead to structural transitions from the fluorite structure, which is the case for some end members of the (U,X)O_2 systems, such as Pu_2O_3, Am_2O_3. The (O/M) ratio is a strong driver of nuclear fuel properties and ultimately of reactor performanceand safety. An accurate determination of the oxygen stoichiometry of mixed oxides U1yMyO2±x is hence crucial, along with a detailed understanding of the nature of the charge compensating defects and their effects on the local structure.

UO_2 and mixed oxides have been extensively experimentally studied with numerous techniques like X-ray diffraction (XRD) for the structural parameters or X-ray absorption spectrocopy (XAS) to explore the electronic and local environments of the different atoms. One of the experimental techniques permitting the investigation of vacancy defects created by irradiation is positron annihilation spectroscopy (PAS). Neutral or negative vacancies can trap positrons and changes the lifetime of positrons compared to the bulk material. PAS was applied on UO_2[2–4] and calculations were performed to assist the interpretation of the results[4].

Since experimental studies are particularly technically challenging and costly on actinide-bearing materials, theoretical studies are required to complement them and give some insight on the underlying phenomena. To this end, density functional theory (DFT) is the method of choice, but a special treatment is required to take into account the strong correlations between the f electrons. Among these treatments, the DFT+U[5] method has shown great success without an increase of the computational time.

UO_2 have been extensively studied with atomic calculations as DFT+U[5–16] or empirical potentials[17–24]. PuO_2 have also been investigated with DFT+U calculations[25] and more recently, CeO_2[26] and AmO_2[27]. Several structural and defect properties of La_2O_3 have been calculated[28] and do not require a $+U$ treatment since there is no f electron in La. Calculations on mixed oxides are scarcer and have only been performed in the past few years with DFT. This is due to the fact that they require larger computational resources to reproduce the chemical disorder by using large enough supercells. Structural and electronic properties of uranium–plutonium and americium mixed oxides have been studied by DFT++U[29, 30], but the defect properties were not investigated (except for the oxy-

gen monovacancy in (U,Am)O_2). (U,Ce)O_2. The cation charge states and formation enthalpies were studied with DFT+U in U-La and U-Ce mixed oxides but with small supercells[31, 32].

Here we propose a comparative theoretical study of several mixed oxides (U,X)O_2 with X=La, Ce, Pu, Am, to understand the differences and similarities of UO_2 doped with trivalent and tetravalent elements in the presence of vacancies and for structural and energetic properties. First we examine the effect of the doping on the structural parameter of the fluorite structure with and without oxygen vacancies and we compare our results with experimental values obtained with X-ray diffraction. Then we calculate the formation energies of several vacancy defects and their associated positron lifetime.

This paper is organized as follows: in the next session we will carefully present and discuss the different aspects of the methodology that we use to calculate the electronic structure of the (U,X)O_2 compounds, the formation energy of various vacancies and the positron lifetime associated to those point defects, then we will present the results and discuss the differences between the considered compounds before giving a conclusion.

II. COMPUTATIONAL SCHEME

A. Computational parameters

Ab initio simulations were performed using the ABINIT package[33–35] in the framework of the Projector Augmented Wave (PAW) method[36, 37] and by means of the generalized gradient approximation (GGA) according to the parametrization of Perdew, Burke and Ernzerhof (PBE) for the exchange-correlation energy and potential [38]. Results are obtained using a plane-wave cutoff energy equal to 600 eV. According to our convergence tests, this input parameter lead to a precision lower than 1 meV per atom for energy differences. 96 atoms supercells ($2 \times 2 \times 2$) are used. The calculations are done on a $2 \times 2 \times 2$ k-points mesh generated by the Monkhorst–Pack[39] method, which is sufficient for an energy convergence less than 0.3 meV per atom. As in other studies on these systems[27, 29, 30] we neglect the spin-orbit coupling (SOC). Firstly because the additional computational time would prevent the use of supercells sufficiently large for an accurate description of disorder and defects and secondly because it has been shown that SOC have a negligible impact on the ground state and defect properties. Moreover, to simulate magnetism, we used the longitudinal 1k AFM order which, without including SOC, is more stable than the transverse 3k AFM order[27, 29].

TABLE I. U and J parameters used in the GGA+U calculations for the different cations studied here.

cation	U (eV)	J (eV)
La	0.0	0.0
Ce	5.0	0.0
U	4.5	0.54
Pu	4.0	0.7
Am	6.0	0.75

B. DFT+U method

In order to take into account the strong correlations between the f electrons in actinides and lanthanides cations (Ce, La has no f electrons), a Hubbard-like term is added by means of the DFT+U Liechtenstein scheme[40]. The (U, J) parameters for the different cations are given in table. I. These values are similar to previous DFT+U calculations by Shi *et al.* on CeO_2[26], Jomard *et al.*[25] on PuO_2, Dorado *et al.*[10] on (U,Pu)O_2, Talla Noutack *et al.*[27] on AmO_2 and (U,Am)O_2[30].

To search for the ground state with the DFT+U method, we applied the occupation matrix control scheme[25, 41] on the f orbitals and fully relaxed the supercells. Our methodology is similar to the one proposed by Talla Noutak *et al.*[30] to study (U,Am)O_2 mixed oxides. As a starting point we used the f occupation matrices orbitals and the corresponding valence states (IV+) of the end members UO_2, CeO_2, PuO_2 and AmO_2, except for (U,La)O_2 where we used the occupation matrices for U^{V+}. For the twenty first steps of the self-consistent cycles the occupation matrices are kept fixed, then the constraint is lifted and the system fully relaxed allowing possible electronic charge transfers which induce changes in the atomic valence states.

The relaxation of the positron was performed using the TCDFT[42, 43], precisely in the Puska Seitsonen and Nieminen parametrization[44] with the gradient correction referred as PSN+GC[4] and as implemented in the ABINIT package[45]. The choice of the PSN+GC scheme was made on the basis of the previous work on UO_2[4].

C. Systems and stoichiometry regimes studied

The defect calculations were performed using a supercell containing 96 atoms, i.e., by doubling the conventional cell along the three lattice parameters, which is a standard supercell also used in previous work on defects[11, 26] and mixed oxides[29, 30]. Doping atoms were distributed following the special quasirandom structure (SQS) method[46], again following previous works on mixed oxides[29, 30].

Several vacancies defects were studied in our work: the monovacancies V_O and V_U, divacancies $2V_O$ and $2V_U$, the $3V_O$ and $4V_O$ vacancies. The V_O, $2V_O$, $3V_O$ and

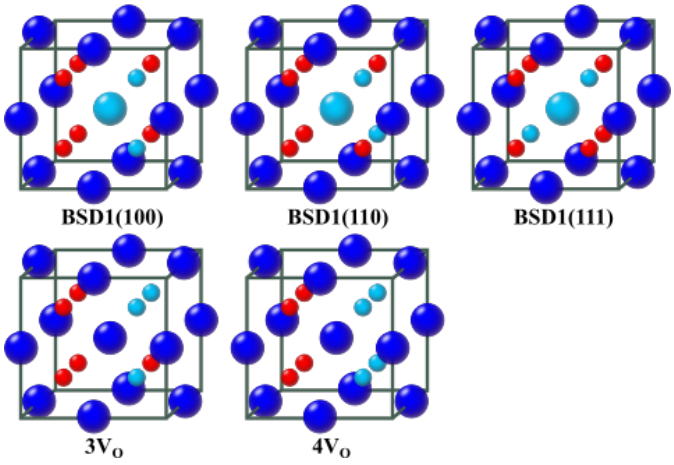

FIG. 1. Vacancy clusters studied in this work, bound Schottky defects, 3 and 4 O vacancies. The bound Schottky defects corresponds to one UO_2 vacancy and are defined by the angle between the two O vacancies: BSD1 with O vacancies along the (100) direction, BSD2 with O vacancies along the (110) direction; and BSD3 with O vacancies along the (111) direction.

$4V_O$ correspond to (O/M) ratios of 1.969, 1.938, 1.906 and 1.875 respectively. $3V_O$ is formed by first nearest neighbors oxygen monovacancies forming a triangle and $4V_O$ by adding an oxygen monovacancy to $3V_O$ forming a rectangle, see Fig. 1. We also studied the bound Schottky defects (BSD), consisting of one UO_2 vacancy, with one U vacancy and two adjacent O vacancies. Depending of the positions of the two O in the U-centered oxygen cage, there is three BSDs: with the two vacancies aligned along (100), (110) and (111) directions, named BSD1, BSD2 and BSD3, respectively, see Fig. 1. In the case of the neutral defects, we removed certain atoms to create vacancies. To obtain charged defects, we further added or removed a given number of electrons in the supercell (e.g., we removed one uranium atom and added four electrons to obtain the V_U^{IV-} vacancy). Especially, we considered the defect charges for which the formal charge of uranium and oxygen ions in UO_2 (O^{II-} and U^{IV+}) is conserved since these charges were found in previous works to be the most stable ones for Fermi levels close to the middle of the band gap[11, 47].

Since we are studying mixed oxides with SQS, the positions of the vacancies are no longer equivalent as they would be in UO_2. For example for a O vancancy we should consider the 64 O positions in the 96 atoms supercell and compared the energies. We did not perform all these calculations but we will discuss this effect for the (U,La)O_2 system.

D. Formation energy of charged vacancies

The formation energy of a defect represents the variation between the total energy of the perfect crystal and the energy of the supercell containing the defect, plus some correction terms relative to the charge. We use the general expression of the formation energy for a defect V_X^q in the charge state q, $E_{\rm form}(V_X^q)$, defined as[26, 48]:

$$E_{\rm form}(V_X^q) = E_{\rm tot}(V_X^q) - (E_{\rm tot}({\rm bulk}) - \sum_i n_i\mu_i) + q(\mu_e + E_{\rm homo}) + E_{\rm corr} \quad (1)$$

where $E_{\rm tot}(V_X^q)$ is the total energy of the supercell containing the charged defect V_X^q, and $E_{\rm tot}({\rm bulk})$ is the total energy of the perfect bulk supercell. n_i is the number of atoms of the i type added to or removed from the bulk, and μ_i is the chemical potential of the i atom. μ_e is the electron chemical potential which varies in the band gap. $E_{\rm homo}$ is the energy of the valence band in the bulk. $E_{\rm corr}$ is the correction energy due to the finite size of the supercell containing the Madelung term $\Delta E_{\rm el}$ to correct the interaction with periodic images[49, 50] and an alignment potential $\Delta\nu$ to correct the shifted band structure between the defect and the perfect supercell:

$$E_{\rm corr} = \Delta E_{\rm el} + q\Delta\nu \quad (2)$$

with

$$\Delta E_{\rm el} = (\alpha q^2)/(2\epsilon_0 L) \quad (3)$$

$$\Delta\nu = \langle\nu_{\rm KS}^{\rm bulk}\rangle - \langle\nu_{\rm KS}^{\rm defect}\rangle \quad (4)$$

α is the Madelung lattice constant which is 2.519 for the fluorite structure[53] and ϵ_0 is the dielectric constant which is 22 for UO_2[54]. L is the length of the supercell edge for the bulk. $\langle\nu_{\rm KS}^{\rm bulk}\rangle$ and $\langle\nu_{\rm KS}^{\rm defect}\rangle$ are the average Kohn-Sham potentials for the bulk and the defected supercell, respectively.

Since the defects considered in our work are formed by oxygen and uranium atoms, the chemical potentials μ_i in Eq.1 correspond to the oxygen and uranium chemical potentials in (U,X)O_2, denoted $\mu_{\rm O}^{\rm (U,X)O_2}$ and $\mu_{\rm U}^{\rm (U,X)O_2}$, respectively. These quantities are not given by the DFT+U calculations since they depend on the stoichiometry and the partial pressure of oxygen. In order to obtain them, we use a method based on the study of Na-Phattalung et al.[51] and Hong et al.[52], considering the standard enthalpy of formation for various phases of the U-X-O systems. For (U,X)O$\equiv {\rm U}_{1-y}{\rm X}_y{\rm O}_{2\pm x}$, it is defined as

$$\Delta H_f^{\rm (U,X)O} = \mu_{\rm (U,X)O}^{\rm bulk} - (1-y)\mu_{\rm U}^{\rm met.} - y\mu_{\rm X}^{\rm met.} - 2\mu_{\rm O}^{\rm O_2} \quad (5)$$

where $\mu_{\rm U}^{\rm met.}$ and $\mu_{\rm X}^{\rm met.}$ are respectively the chemical potential for one U atom and one X atom in their standard metallic state, and $\mu_{\rm O}^{\rm O_2}$ is the chemical potential for one O atom in the O_2 gaseous molecule. $\mu_{{\rm U}_{1-y}{\rm X}_y{\rm O}_2}^{\rm bulk}$ is a constant defined by:

$$\mu^{\rm bulk}_{\rm (U,X)O} = (1-y)\mu^{\rm (U,X)O}_{\rm U} + y\mu^{\rm (U,X)O}_{\rm X} + 2\mu^{\rm (U,X)O}_{\rm O} \quad (6)$$

Inserting Eq.6 into Eq.5, and introducing the relative chemical potentials:

$$\Delta\mu_{\rm U} = \mu^{\rm (U,X)O}_{\rm U} - \mu^{\rm met.}_{\rm U} \quad (7)$$

$$\Delta\mu_{\rm X} = \mu^{\rm (U,X)O}_{\rm X} - \mu^{\rm met.}_{\rm X} \quad (8)$$

$$\Delta\mu_{\rm O} = \mu^{\rm (U,X)O}_{\rm O} - \mu^{\rm O_2}_{\rm O} \quad (9)$$

we can rewrite the enthalpy of formation of (U,X)O as:

$$\Delta H_f^{\rm (U,X)O} = (1-y)\Delta\mu_{\rm U} + y\Delta\mu_{\rm X} + 2\Delta\mu_{\rm O} \quad (10)$$

The enthalpies of formation of the mixed oxides are close to the values for the end members. Indeed, the difference between $\Delta H_f^{\rm (U,X)O}$ and $\Delta H_f^{\rm UO_2}$ and $\Delta H_f^{\rm XO_2}$ is given by the mixing enthalpy $\Delta H_{\rm mix}$[29] :

$$\Delta H_f^{\rm (U,X)O} = (1-y)\Delta H_f^{\rm UO_2} + y\Delta H_f^{\rm XO_2} + \Delta H_{\rm mix} \quad (11)$$

For (U,Pu)O_2, the calculated value of $\Delta H_{\rm mix}$ is between 0 and -10 meV[29] while for (U,Am)O_2 it is between 0 and -0.4 eV. Compared to the values for the formation energies, around 10 eV, $\Delta H_{\rm mix}$ can be neglected. Moreover, the experimental values for $\Delta H_f^{\rm XO_2}$ can be approximated to the value of $\Delta H_f^{\rm UO_2} = -11.24$ eV ($\Delta H_f^{\rm XO_2}$ = -11.30, -10.95, -9.66 eV for X=Ce, Pu and Am respectively[53]). Therefore, we can replace $\Delta H_f^{\rm (U,X)O}$ by $\Delta H_f^{\rm UO_2}$.

$$-11.24 < \Delta\mu_{\rm U} < 0({\rm eV}) \quad (12)$$

$$-5.62 < \Delta\mu_{\rm O} < 0({\rm eV}) \quad (13)$$

We will consider three conditions for the chemical potentials, O-poor ($\Delta\mu_{\rm U}$ = 0 eV, $\Delta\mu_{\rm O}$=-5.62 eV), O-rich ($\Delta\mu_{\rm U}$ = −11.24 eV, $\Delta\mu_{\rm O}$=0 eV) and the average that should be close to the stoichiometric conditions ($\Delta\mu_{\rm U}$ =-5.62 eV, $\Delta\mu_{\rm O}$=-2.81 eV)

III. RESULTS

A. Pure oxides

First we discuss our results for XO_2 (X≡ U, Ce, Pu, Am) in the fluorite structure and the hexagonal structure for the sesquioxide La_2O_3. In table II we show our values for the lattice parameters and the band gap obtained with PBE+U with a comparison with previous theoretical values using similar calculations scheme and experimental data. Concerning the gap, UO_2 is known to be a Mott insulator, the band gap being between U $5f$ bands, while CeO_2, La_2O_3, PuO_2 and AmO_2 are charge-transfer insulators with a gap between O $2p$ and f states. As expected our values are in close agreement with previous theoretical works. We slightly overestimate the lattice parameters compared to experiments. These values will be use to obtain the Vegard's law for the (U,X)O_2 systems.

TABLE II. Calculated lattice parameters and band gaps of the fluorite structure of XO_2 (X≡ U, Ce, Pu, Am) and the hexagonal structure of La_2O_3 (the first and the second values correspond to a and c respectively). Previous theoretical results and experimental data are listed for comparison.

oxide	method	a(Å)	Gap (eV)
UO_2	PBE+U	5.54	2.68
	PBE+U[29]	5.54	2.50
	Exp.[54, 55]	5.47	2.1
La_2O_3	PBE	3.95, 6.19	3.8
	PBE[56]	3.93, 6.15	3.8
	Exp[57, 58]	3.94, 6.13	5.5
CeO_2	PBE+U	5.50	2.6
	PBE+U[26]	5.49	2.7
	Exp.[59–61]	5.41	3.0
PuO_2	PBE+U	5.44	2.1
	PBE+U[29]	5.45	2.0
	Exp.[54, 62]	5.40	1.8
AmO_2	PBE+U	5.43	1.1
	PBE+U[27]	5.44	1.1
	Exp.[63, 64]	5.37	1.3

B. Electronic structure

To understand the electronic structure of the mixed oxides studied here, the projected density of states (DOS) of $U_{0.75}X_{0.25}O_2$ (X≡ Ce, Pu, La, Am) were calculated and are presented in figure 2 with the DOS of UO_2 for comparison. The top of the valence band was set as the reference energy (0 eV). Our result for UO_2 is close to previous results[65], the gap in UO_2 is between U f states. We first notice that all the oxides display an insulating character and that the gap in the mixed oxides (between 1.1 and 1.5 eV) is lower than the one found in UO_2 (2.7 eV). We also observed that the f states of U IV+ are almost unchanged in the mixed oxides compared to UO_2, regardless of the other cationic species, with a gap between these states around 2.5 eV (blue in fig. 2). But while the top of the valence band is always dominated by the U^{IV+} $5f$ states, we observe the appearance of other states at the bottom of the conduction band which narrow the gap. The nature of these states depends on the oxidation state of the cation associated

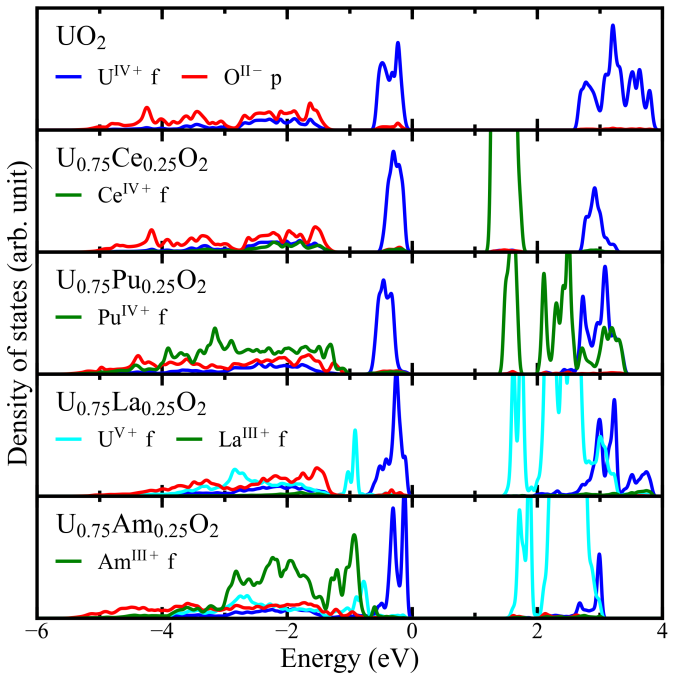

FIG. 2. The projected DOS of U^{IV+}, U^{V+}, Ce^{IV+}, Pu^{IV+}, La^{III+}, Am^{III+}, and O^{II-} components in UO_2 and $U_{0.75}X_{0.25}O_2$ (X≡ Ce, Pu, La, Am) and computed by DFT+U. For better comparison the energies have been shifted so that 0 eV corresponds to the highest occupied state.

TABLE III. Ionic radius of the cation considered in this work

cation	radius(Å)
La^{III+}	1.18
Ce^{III+}	1.14
Ce^{IV+}	0.97
U^{III+}	1.17
U^{IV+}	1.03
U^{V+}	0.90
Pu^{III+}	1.00
Pu^{IV+}	0.96
Am^{III+}	1.09

with U. For Ce and Pu, which are IV+ as U atoms in UO_2, the band gap is formed between U f states and Ce and Pu f states (green in fig. 2). For La and Am, which are trivalent, the band gap is formed between U^{IV+} and U^{V+} f (cyan in fig. 2) states.

C. Lattice parameter

In this section we study the evolution of the lattice parameter of $(U,X)O_{2-x}$ as a function of X contents for the stoichiometric, $x = 0$ and hypostoichiometric, $x \neq 0$ cases. In our 96 atoms supercell we remove up to four oxygen atoms corresponding to $2-x \sim 1.969, 1.938, 1.906$ and 1.875 for one, two, three and four oxygen vacancies respectively. Our results are compared to experimental data and the linear evolution of the lattice parameter with respect to the composition, known as Vegard's law[66]. The lattice parameter will be presented as the relative variation Δa with respect to the one in pure UO2 :

$$\Delta a(\%) = \frac{a_{(U,X)O_2} - a_{UO_2}}{a_{UO_2}} \qquad (14)$$

Our results are given in table IV for all the cases studied in our work.

1. $ULaO_2$

La is trivalent, and under oxygen atmosphere forms the sesquioxide La_2O_3. In stoichiometric conditions, the doping of UO_2 with La ions should induce the oxidation of the same amount of U^{IV+} to U^{V+} and an increase in the cell parameter since the ionic radius of La^{III+} is much larger than that of U^{IV+} and this contribution is not entirely compensated by the uranium oxidation (see table III).

In our calculations we clearly observe that at the concentrations considered here, up to 50% of La, all the La atoms are La^{III+} with the same number of uranium atoms being oxidized in U^{V+}, the rest staying U^{IV+}. This behaviour is similar to the one observed in a recent theoretical study of $(U,Am)O_2$[30] and the experimental conclusions of D. Prieur *et al.* on $(U,La)O_2$[1]. Using X-ray absorption near edge spectroscopy (XANES) and X-ray diffraction to assess the stoichiometry of several $(U,La)O_2$ solid solutions, they observed that U^{V+} is formed in quasi-equimolar proportion as La^{III+} confirming the absence of oxygen vacancies. We present in Fig. 3 our results for the variation of the lattice parameter of $(U,La)O_2$ compared to that of UO_2. As expected, we observe an increase of the lattice parameter with the La content.

We also compare in Fig. 3 our results with experimental data[1, 57, 68–73]. There is a strong dispersion of the measures that can be attributed to deviations from stoichiometric composition, either in the hypo or hyper-stoichiometric regimes (blue[71] and green[57, 68, 73] symbols respectively in Fig. 3). The results of D. Prieur *et al.*[1] and several other studies claiming to have achieved (O/M) ratio equals to 2.0[69, 70, 72] are in red symbols in Fig. 3. The red dashed line is the line separating the hypo and hyper-stoichiometric regimes as proposed by D. Prieur *et al.*[1]. Surprisingly, the study of Z. Talip *et al.*[68] (as the one of R.Venkata Krishnan *et al.*[57]) where they discuss the presence of oxygen vacancies in UO2 with 6, 11, 22 mol% lanthanum in relation with an extra band in their Raman spectra at ∼540 cm^1, are close to this red line and not above. This could indicate a misinterpretation of the Raman spectra and difficulties to measure the (O/M) ratios[1].

TABLE IV. Lattice parameter (in Å) of the mixed oxides as a function of the dopant content and for several vacancies.

	a(Å)										
	UO_2	$ULaO_2$			$UCeO_2$		$UPuO_2$			$UAmO_2$	
Defect	-	6.25%La	12.5%La	25%La	6.25%Ce	25%Ce	6.25%Pu	25%Pu	50%Pu	6.25%Am	25%Am
-	5.537	5.539	5.543	5.554	5.535	5.527	5.532	5.515	5.484	5.532	5.518
V_O	5.541	5.549	5.552	5.561	5.547	5.536	5.541	5.524	5.497	5.540	5.527
$2V_O$	5.543	5.550	5.564	5.573	5.547	5.552	5.541	5.532		5.541	5.538
$3V_O$	5.549	5.555	5.565	5.580	5.552	5.567	5.546	5.545		5.546	5.552
$4V_O$	5.558	5.559	5.572	5.588	5.561	5.577	5.555	5.554		5.554	5.555
V_U		5.529	5.535	5.541	5.520	5.512	5.520	5.500	5.472	5.518	5.506
$2V_U$		5.519	5.522	5.542	5.511	5.503	5.508	5.486		5.511	5.503
BSD1		5.547	5.550	5.565	5.542	5.532	5.539	5.518	5.490	5.542	5.525
BSD2		5.551	5.551	5.563	5.541	5.535	5.538	5.518	5.484	5.540	5.531
BSD3		5.548	5.549	5.566	5.539	5.529	5.535	5.517	5.490	5.539	5.532

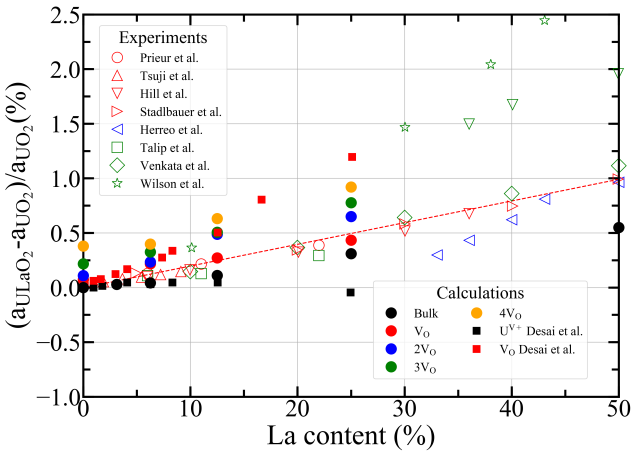

FIG. 3. Variation of the calculated[67] and experimental[1, 57, 68–73] lattice parameter of (U,La)O_2 compared to that of UO_2. The filled circles are our results as a function of the La content and the number of oxygen vacancies in the 96 atoms supercell (hypostoichiometric solid). The red dashed line is supposed to correspond to stoichiometric conditions as proposed by D. Prieur *et al.*[1]. The experimental data are divided in three groups : red: stoichiometric conditions, blue: hyperstoichiometric conditions and green: hypostoichiometric conditions. The data of D.C Hill[69] are in red and green. Our calculations are the filled colored circles, the black and red squares are the calculations of K. H. Desai *et al.*[67] with an empirical potential with the incorporation of U^{V+} and oxygen vacancies to compensate the charge of the La accomodation.

Our calculated lattice parameter for the bulk material are close to the red line at low La content but start to deviates from this line above 10% of La. The discrepancies are small at 12.5 and 25%, around 0.2% and can be explained by the uncertainties in the calculations and the experiments, but at 50%, they are much larger, around 0.5%. This could be due to deviation from stoichiometry, oxygen vacancies increase the volume, see below. An other possibility is that we only considered the fluorite structure, but the end member, La_2O_3, has an hexagonal structure and it is possible that this phase is present in the experiments for 50% of La content.

K. H. Desai *et al.*[67] performed calculations with empirical potential, testing two charge compensation mechanisms for La accommodation, the incorporation of U^{V+} and oxygen vacancies. They found that the volume was almost independent with U^{V+}, and a strong augmentation with the oxygen vacancies. Therefore they proposed a mechanism consisting of an equal mix of oxygen vacancies and U^{V+}. Our ab-initio calculations do not support this solution.

Our results for supercells with oxygen vacancies shows a increase of the volume when the (O/M) ratio decreases. This is in agreement with the experimental results and the calculations of K. H. Desai *et al.*[67]. We also notice that the increase in volume is greater when the La content increases. We have also tested the position of the oxygen vacancy inside the supercell for 6.25% La (2 La atoms in the 96 atoms supercell). There is almost no difference in terms of volume when the vacancy has two La atoms in the first neighbors shell or only uranium atoms, +0.22% and +0.20% respectively.

2. *UCeO$_2$*

Cerium is often used in simulation studies of plutonium because of their similar chemical and thermodynamic behavior, with the advantage that Ce has no radiotoxicity issue compared to Pu. The phase diagrams of (U,Ce)O_2 and (U,Pu)O_2 are also similar with an homogeneous region of the solid solution with the fluorite structure.

We present in Fig. 4 our results and experimental data for the variation of the lattice parameter of (U,Ce)O_2 compared to that of UO_2. Contrary to the doping with La, we observe a decrease of the lattice parameter with the Ce content. At the end of our simulations, the Ce and U atoms are in the valence state +IV. Therefore the volume decrease can be explained by the lower value of the Ce^{IV+} ionic radius compared to the one of U^{IV+}, see table III. Our values for the bulk material are perfectly

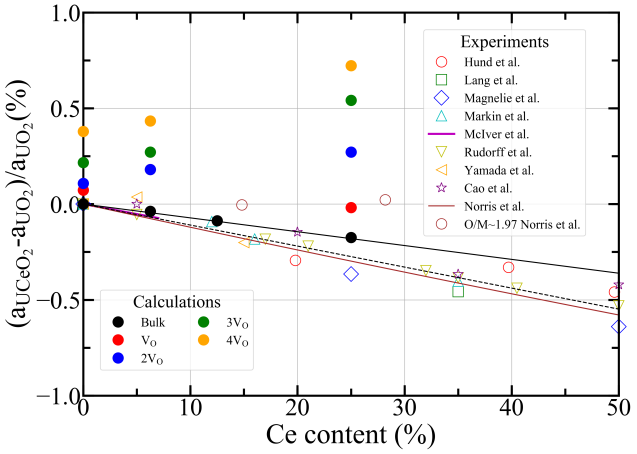

FIG. 4. Variation of the calculated and experimental[74–81] lattice parameter of (U,Ce)O_2 compared to that of UO_2. The filled circles are our results as a function of the Ce content and the number of oxygen vacancies in the 96 atoms supercell (hypostoichiometric solid). The theoretical and experimental Vegard's law are the solid and dashed black lines respectively. The red line is a least-squares parabolic fit of their experimental data proposed by D. Norris and P. Kay[82].

aligned with the theoretical Vegard's law (a straight line between the lattice parameter of the end members UO_2 and CeO_2, in black on Fig. 4). Most of the experimental values follows also the Vegard's law (red line in Fig. 4). The difference between the theoretical and experimental Vegard's law comes from the stronger overestimation of the lattice parameter of CeO_2 (+0.09 Å) compare to UO_2 (+0.07 Å), see table II. D. Norris and P. Kay[82] performed a least-squares parabolic fit of their data (the red line in Fig. 4 which is really close to the Vegard's law. They also obtained some values with an estimated (O/M) ratio of 1.97 which in our calculations correspond to a supercell with one oxygen vacancy. As for La we observe an increase in volume in the hypostoichiometric conditions and the increase is larger with the Ce content. When we remove oxygen atoms from the supercell, the Ce atoms (two for each removed oxygen) change their charge state from IV+ to III+ to compensate the charge. If there is not enough Ce atoms, the U atoms take over. The ionic radius of Ce^{III+} being larger that Ce^{IV+}, this can explain the volume increase. This can also explain that with higher Ce content, the increase is more important since the ionic radius difference between Ce^{III+} and Ce^{IV+} is larger than U^{III+} and U^{IV+}.

3. $UPuO_2$

We present in Fig. 5 our results for the variation of the lattice parameter of (U,Pu)O_2 compared to that of UO_2. As for (U,Ce)O_2 our values follow the Vegard's law, in agreement with the experiments[54, 83]. We found a smaller overestimation of PuO_2 volume compared to UO_2 which explains why we predict a steeper slope for the Vegard's law in comparison with the experimental one. As expected our calculations are in excellent agreement with similar calculations of I. Njifon *et al.*[29] while they differ from the calculations performed with empirical potentials fitted on experimental data[20, 84]. As for Ce doping, we found a volume contraction with the Pu content which again, can be explained by the ionic radius difference between U^{IV+} and Pu^{IV+}. In our simulations and for the bulk material, Pu atoms are only found in the IV+ charge state.

As for the two previous cases, La and Ce doping, we found an increase of the lattice parameter when we introduce oxygen vacancies in the supercell. The consequences in (U,Pu)O_2 are similar to those observed in (U,Ce)O_2. To compensate the charge in the presence of oxygen vacancies, the Pu atoms change their charge state from IV+ to III+ and if they are not enough (when the number of Pu atoms are inferior to two times the oxygen vacancies) some U atoms becomes III+. This result in an increase of the volume of the supercell due to the difference between the ionic radius.

Due to its technological importance and its use in pressurized water reactors, as MOX fuel, the effect of deviation from stoichiometry on the lattice parameter of (U,Pu)O_2 system has been well studied experimentally[54, 83, 85, 86]. We plot on Fig. 5 the model proposed by M. Kato and K. Konashi[83] for deviation from stoichiometry corresponding to one up to 3 vacancies in our supercell. At 25 and 50% (for the monovacancy) of Pu content, our results are in good agreement with the experimental model while for lower contents we predict a smaller increase of the volume. Obviously, similar agreement and discrepancies are observed with the calculations of C Takoukam-Takoundjou *et al*[84] since their potential were fitted to reproduce the experimental data.

4. $UAmO_2$

We present in Fig. 6 our results for the variation of the lattice parameter of (U,Am)O_2 compared to that of UO_2. As for La, we found the Am atoms with a valence charge state of III+ in our calculations and en equivalent number of uranium changing their charge state from IV+ to V+ to compensate the charge. This in agreement with the calculations of M. Talla Noutack *et al.* [30] and experimental conclusions of D. Prieur *et al.*[87] (up to 20% of Am content).

We observed a small deviation with the Vegard's law, our values are systematically larger. This was already observed by M. Talla Noutack *et al.* [30], specially at 50% of Am content where the deviation culminates at +0.36% between the theoretical volume and the Vegard's law value.

Contrary to the previous cases, La, Ce and Pu, for Am, the discrepancies between our calculations and the

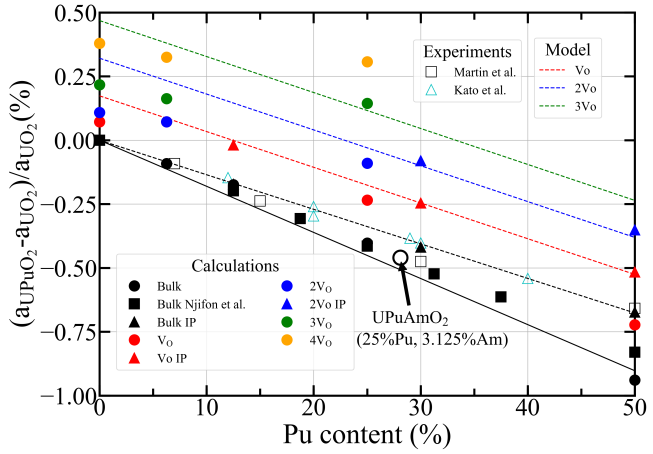

FIG. 5. Variation of the calculated[29, 84] and experimental[54, 83] lattice parameter of (U,Pu)O_2 compared to that of UO_2. The filled circles are our results as a function of the Pu content and the number of oxygen vacancies in the 96 atoms supercell (hypostoichiometric solid). The theoretical and experimental Vegard's law are the solid and dashed black lines respectively. The red, blue and green dashed lines are calculated with the expression proposed by M. Kato and K. Konashi[83]. The black squares are ab-initio calculations with the same approximations as us[29] while the filled triangles are calculations performed with empirical potentials[84].

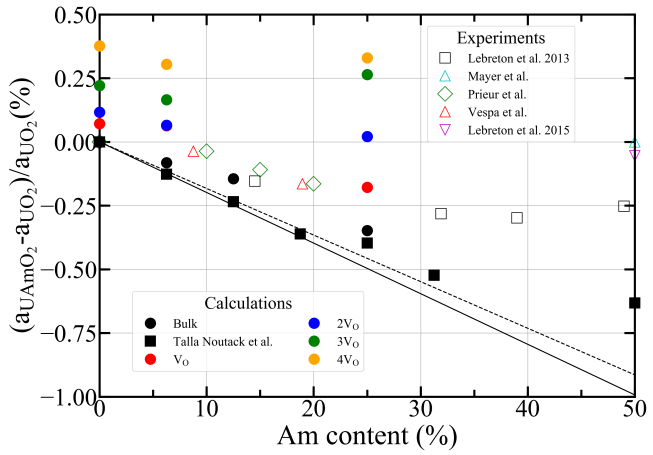

FIG. 6. Variation of the calculated[30] and experimental[88–91] lattice parameter of (U,Am)O_2 compared to that of UO_2. The filled circles are our results as a function of the Am content and the number of oxygen vacancies in the 96 atoms supercell (hypostoichiometric solid). The theoretical and experimental Vegard's law are the solid and dashed black lines respectively.

experimental values are significantly larger. Experimentally, a strong deviation from the Vegard's law is observed[89, 90], a behavior not observed for UO_2 doped with La, Ce and Pu. Several reasons can be at the origin of these discrepancies. It is well known that lattice expansion under self-irradiation effects occur in ^{241}Am-bearing oxides, so the storage period of the sample can have some impact on the measured lattice parameter[90]. An other explanation comes from the charge accommodation mechanism. For Am content up to 20%, D. Prieur *et al.*[87] using XAS and XRD found that the Am^{IV+} is totally reduced to Am^{III+} with equivalent U^{V+}. But more recently, F. Lebreton *et al.*[92] combining XRD, XANES and Raman spectroscopy showed that for $U_{0.5}Am_{0.5}O_{2\pm\delta}$ the number of U^{V+} remains below the amount required for charge balance. They conclude that unlike lower americium contents, this leads to an overall oxygen hypostoichiometry with an average (O/M) ratio of 1.92 (about 2.5 oxygen vacancies in our supercell). We confirm that with oxygen vacancies the lattice parameter increases (as for La, Ce, and Pu). At 25% of Am content we found an increase of $\sim +0.50\%$ compared to the bulk value. This could therefore explain the difference observed between the calculations of M. Talla Noutack *et al.*[30] and the experimental values[91, 92], and confirmed the deviation from the Vegard's law due to hypostoichiometric conditions.

D. Formation energies of vacancies

We present here the results on the formation energies of defects (V_O, $2V_O$, V_U, BSD1 and BSD2) under various charge states, considering three types of stoichiometry conditions. The formation energies are calculated as a function of the Fermi energy in the range of the band gap according to Eq. 1. Depending of the defect considered, uranium, oxygen vacancies or both (BSD) and the dopant of UO_2 the excess or the lack of electron is differently accommodate by the cation. For an oxygen vacancy which is an electrons donor if a tetravalent dopant is present (Ce or Pu), it is reduced from IV+ to III+, while if a trivalent dopant is present (La or Am) it is the U^{V+} that are reduced to U^{IV+}. Uranium vacancies are electrons acceptors, we found that in this case and for all the doping elements, some of the remaining uranium are providing these electrons and therefore oxidize to V+.

Figure 7 show our results for $U_{0.75}X_{0.25}O_2$ (X≡ Ce, Pu, La, Am). For each defect, the most stable charge state depends on the Fermi energy value in the band gap and is given above or below the curves. The stoichiometric conditions do not affect the relative stability of different charge states for the same vacancy. However, the stoichiometric conditions influence the Fermi level position and the relative stability between different vacancies. We also calculate the formation energies of the oxygen vacancies in pure UO_2 (see Fig. 8), especially the oxygen monovacancy which has been much studied[9, 11, 47]. For the Fermi level in the middle of the gap (Fig. 8) we find defects with the formal charge: +2 for V_O and +4 for $2V_O$ as observed in previous works. Our result for V_O are close to those obtain by Vathonne *et al.*[11], except that we observe the neutral state between the charge state +2 and -2. This could be due to the Jahn-Teller matrices that we used in the occupation

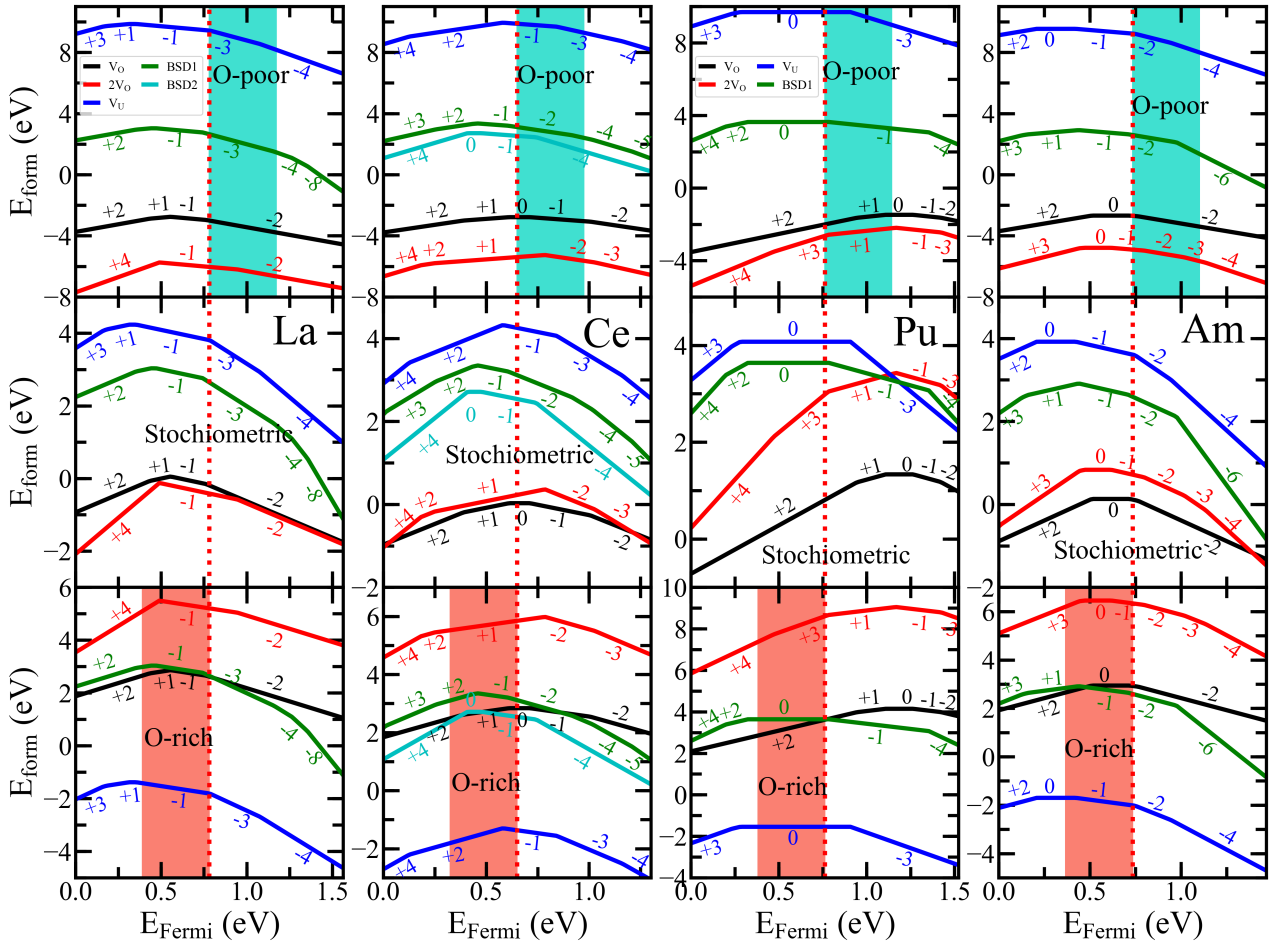

FIG. 7. Formation energy of charged point defects (O monovacancy V_O, in black, O divacancy $2V_O$, in red, U monovacancy V_U, in blue, and bound Schottky defect with the O vacancies along the (100) and (110) direction BSD1 and BSD2, in green and cyan respectively) as a function of the Fermi energy under O-poor conditions (top), stoichiometric (middle) and O-rich conditions (bottom), for UXO_2 with 25% content of X and from left to right : X=La, Ce, Pu and Am.

matrix control scheme but we note that this charge state was previously observed in the works of Crocombette *et al.*[9, 47] without these matrices.

The charge state of the oxygen vacancies strongly depends of the doping element in $U_{0.75}X_{0.25}O_2$, see Fig.7 . In the case of Pu, in the middle of the band gap, we found the charge state +2 and +3 for V_O and $2V_O$ respectively, close to the values obtained for UO_2. For Ce, the charge states have also positive values (0 and +1) but with the trivalent elements, La and Am, the oxygen vacancies have negative charge states (-2). These extra negative charges serve to reduce U^{V+} to U^{IV+}, the ionization state of uranium in pure UO_2. This is an important result, that can be generalized to all the defect studied here. Vacancies in UO_2 doped with trivalent elements, like La and Am have higher charge states than the ones found in UO_2 doped with tetravalent elements like Ce and Pu.

The formation energy of the oxygen di-vacancy is more than two times the formation energy of the mono-vacancy. This indicates that oxygen vacancies will not bound in the system. Of course this result is only valid at 0K, the vibrational entropy contribution at higher temperature could change this result. Recently some results have been obtained on this quantity for actinides systems using either DFT[93–95] or empirical potentials[22] showing that temperature can have a strong impact on the actinides systems properties.

E. Positrons lifetimes

We performed positron lifetime calculations for the fully relaxed defects presented in the previous section with the PSN + GC scheme[4, 44]. The results are presented in Table VI. For almost all types of defects, we considered two charge states. First, we performed positron lifetime (PLT) calculations for neutral defects. Second, we calculated the lifetimes for vacancies in the charge states that were determined as the most stable

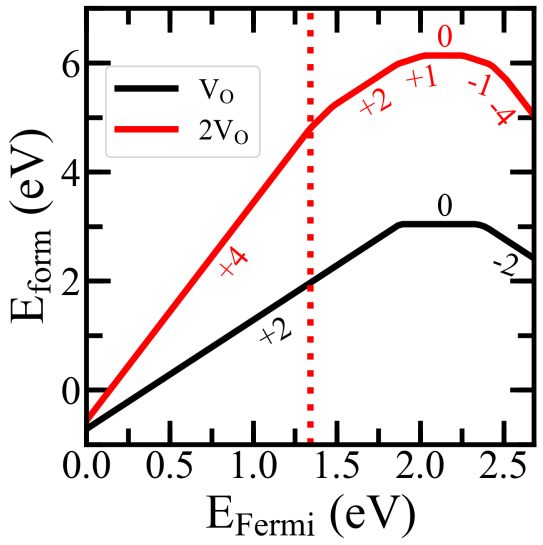

FIG. 8. Formation energy of charged O monovacancy V_O, in black and O divacancy $2V_O$, in red, for UO_2 under stoichiometric conditions.

TABLE V. Calculated positron lifetime for the bulk of the pure oxides.

oxide	Lifetime (ps)
UO_2	162
La_2O_3	174
CeO_2	166
PuO_2	158
AmO_2	159

ones in the stoichiometric material. We would like to emphasize a crucial difference in the procedure to obtain the positron lifetime with the previous work of J. Wiktor *et al.* on UO_2[4]. In our work, first we fully relaxed the supercell with the considered defect and let the atoms adjust their positions and the volume accommodate the vacancy. Then, in a second time, we put the positron in the supercell and relaxed one again the supercell in the presence of the positron to calculate its lifetime. In the previous work of J. Wiktor *et al.*[4] the first step of our scheme is not performed, the positron is placed directly in the perfect structure and the supercell is relaxed in its presence. We believe that our procedure is closer to the positron annihilation spectroscopy, indeed the defects are already present in the studied materials and do not appear when the positron enter the matter. As we will see later in this section, relaxing the supercell before the introduction of the positron can have a strong impact on its calculated lifetime for some defects.

The PLT for all the cases considered in our study are given in Table V for the pure oxides and in table VI for UXO_2. Before going into the details of our results we would like to give the main points that we have learned from these data: (i) the positron lifetime is almost independent of the doping element (at least for the concentrations considered here) , meaning that the lifetime is essentially related to the free volume available, (ii) for uranium vacancies the positron is always trapped while for oxygen vacancies the trapping seems to depend of the surrounding cation oxidation states, (iii) different defects have similar positron lifetimes, consequently the defect identification in the positron annihilation spectroscopy studies is extremely challenging.

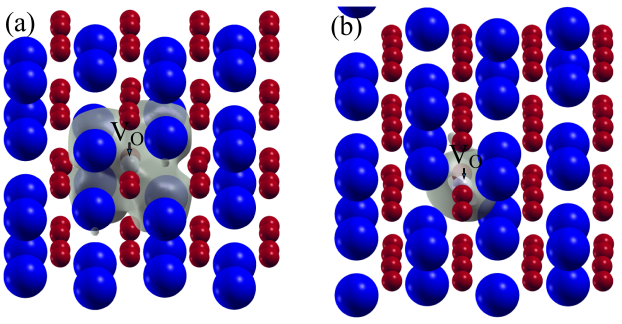

FIG. 9. Positron isodensities (30% of the maximum density) in transparent gray, with a neutral oxygen vacancy in UO_2. Uranium atoms are presented in blue, oxygen atoms in red. Gray spheres represent the oxygen vacancy. (a) the atomic positions were relaxed in the presence of the oxygen vacancy before the introduction of the positron. (b) the atomic positions were relaxed in the presence of the oxygen vacancy after the introduction of the positron as in Ref. [4]. Figures were generated using the XCRYSDEN program[96, 97].

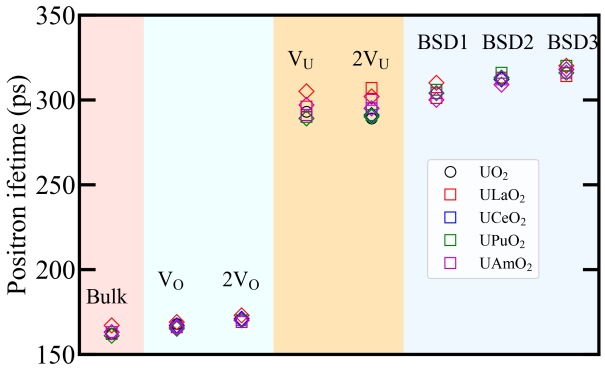

FIG. 10. Positron lifetime for bulk and charged defects for UO_2 in black open circles, UXO_2, X=La, Ce, Pu and Am, in red, blue, green and magenta respectively. The squares and diamond are for 6.25 and 25 % of X atoms content.

The PLT of the 5 oxides that we have considered are close to each other (see table V, especially the dioxides with values ranging from 166 ps for CeO2 to 158 ps for PuO_2, the sesquioxide La_2O_3 having a slightly larger PLT at 174 ps. The PLT of bulk UO_2 and vacancies and several cluster vacancies in UO_2 have already been calculated by J. Wiktor*et al.*[4] (see the red values in table VI) using the same implementation of TCDFT [45] as in our work. For bulk UO_2 we find a value of 162 ps, close to the previous result of 167 ps, the slight difference be-

TABLE VI. Positron lifetimes (in ps) calculated for fully relaxed neutral and charged defects in UXO_2. For each defect, the second line indicates the lifetime and the charge of the most stable charge state of the defect. If there is no number in the second line, the neutral state is the most stable one. The bold numbers indicate the lifetime of the most stable state, whether neutral or charged. For UO_2 the lifetime in red are the results of J. Wiktor *et al.*[4].

	τ(ps)										
	UO_2	$ULaO_2$			$UCeO_2$		$UPuO_2$			$UAmO_2$	
Defect	-	6.25%La	12.5%La	25%La	6.25%Ce	25%Ce	6.25%Pu	25%Pu	50%Pu	6.25%Am	25%Am
-	162 167	**163**	**164**	**167**	**163**	**163**	**162**	**161**	**160**	**163**	**163**
V_O	168 199	**166**	167	170	**166**	**167**	166	165	**164**	166	166
	166 (II+)		**167** (I-)	**169** (II-)			**166** (II+)	**165** (II+)			
$2V_O$	222	226	**171**	**173**	227	170	224	170		224	170
	170 (IV+)	**170** (II+)			**170**(II+)	**171** (I+)	**170** (IV+)	**170** (III+)		**169** (II+)	**170** (I-)
V_U	304	301	300	307	299	299	300	299	299	299	299
	293 (IV-)	**296** (II-)	**296** (II-)	**305** (I-)	**290** (IV-)	**289** (IV-)	**290** (III-)	**289** (IV-)		**291** (IV-)	**297** (II-)
$2V_U$	318	307	307	315	310	303	306	304		310	301
	289 (VIII-)	**307** (II-)	**301** (III-)	**302** (V-)	**295** (IV-)	**291** (V-)	**291** (V-)	**290** (VI-)		**300** (VI-)	**295** (IV-)
BSD1	**304**	304	306	317	**306**	306	**306**	**304**	**304**	308	305
		301 (II-)	**304** (I-)	**310** (III-)		**304** (II-)				**304** (II-)	**300** (II-)
BSD2	**313**	316	312	322	**316**	315	**316**	**313**	**310**	316	314
		313 (I-)	**308** (II-)	**313** (II-)		**312** (I-)				**312** (II-)	**309** (I-)
BSD3	**316**	321	318	326	320	**318**	**320**	**316**	**315**	320	321
		314 (II-)	**310** (III-)	**320** (II-)	**318** (I-)					**316** (I-)	**318** (II-)

ing certainly due to the occupation matrices that we used (obtained with the Jahn-Teller distortion). However for the oxygen monovacancy we find a lifetime close to the bulk value, only slightly longer (166 vs 162 ps), in stark contrast with the previous value of 199 ps[4]. We expect that this discrepancy comes from the relaxation scheme that we used as mentioned previously. To understand these differences we plot in Fig. 9 the isodensities of the positron calculated with both schemes. If the positron is introduced in the perfect supercell with an oxygen vacancy as in J. Wiktor *et al.*, the positron is localized inside the vacancy (see 9.b) , while if the positron is introduced after the supercell relaxation its localization is different. it is only partially localized in the oxygen vacancy. We clearly see in figure 9.a that the positron also localized between the neighboring uranium atoms. The positron lifetime being inversely proportional to its density (also to the electron one)[45], this explain the shorter lifetime found with our scheme compared to the one used by J. Wiktor *et al.*[4]. For the other defects (V_U, $2V_U$ and BSDs) our results for the mixed oxides are in excellent agreement with the values obtained by J. Wiktor *et al.* for pure UO_2. This seems to indicate that in these cases, relaxing the supercell before the introduction of the positron has a negligible effect.

In overall, the doping of UO_2 with the four elements and up to 25% amount considered in our work has a marginal impact on the positron lifetime. This can be clearly seen on Fig. 10 where we plot the positron lifetime for bulk UO_2 and mixed oxides and for the most stable charge state of the defects. It is only dependant of the type of defect present in the supercell. We also observe that the positron lifetime with one and two oxygen

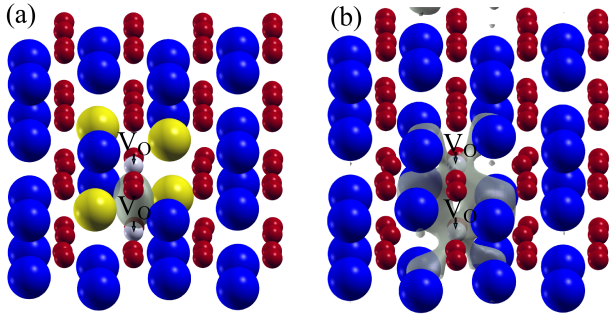

FIG. 11. Positron isodensities (70% of the maximum density) in transparent gray, with a two oxygen vacancies in UO_2 for (a) the neutral charge state and (b) the formal charge state +IV. Uranium III+ and IV+ atoms are presented in yellow and blue respectively, oxygen atoms in red. Gray spheres represent the oxygen vacancies. Figures were generated using the XCRYSDEN program[96, 97].

vacancies are really close to the bulk value. For $2V_O$ the neutral charge state has in some cases a larger value (for UO_2, and the mixed oxides with 6.25 % atoms content, see table VI), around 225 ps. If we plot the positron isodensities for one of these cases, see Fig.11.a, we observe that the positron is well localized between the two oxygen vacancies. But in the stable charge state, see Fig.11.b, the positron is between the adjacent uranium atoms and the positron lifetime is therefore close to the value for the bulk material where it is delocalized in the entire supercell. It seems that the trapping of the positron in the volume created by the oxygen vacancies is related to the presence of U^{III+}. For 6.25 X atoms % there is not

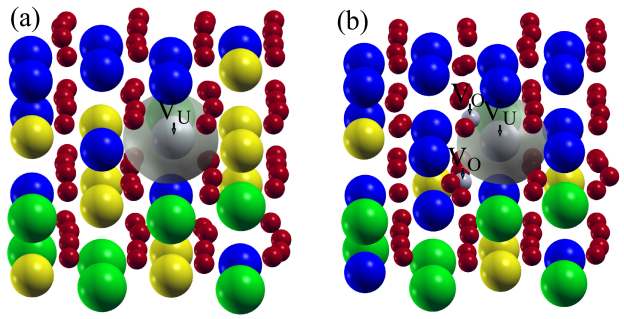

FIG. 12. Positron isodensities (30% of the maximum density) in transparent gray in $U_{0.75}La_{0.25}0_2$ for an uranium vacancy in the charge state I- (a) and the bound Schottky defect BSD1 in the charge state III- (b). Uranium IV+ and V+ atoms are presented in blue and yellow respectively, oxygen atoms in red, La III+ in green. Gray spheres represent the oxygen and the uranium vacancies. Figures were generated using the XCRYSDEN program[96, 97].

enough U^{V+} (X=La, Am) or X^{IV+} to accommodate the 4 extra electrons provide by the two oxygen vacancies, so two U^{IV+} are reduced to U^{III+} (compared to four in pure UO_2).

For uranium vacancies and BSDs the lifetime is much larger than for the bulk material. As shown in Fig. 12 the positron is localized inside the uranium vacancy and the oxygen vacancies seems to have a negligible effect on the density and the lifetime. Indeed the lifetime for the BSDs are only slightly larger ($\sim 3\%$) than the one found for the uranium vacancies. This is in agreement with the conclusions of J. Wiktor *et al.* for UO_2[4]. We also remark that the lifetimes of the negative defects are always shorter than for the neutral ones. This is due to a higher electronic density in the negatively charged defects. Uranium vacancies and BSDs have almost the same positron lifetime but while the uranium vacancies are always negatively charged, the BSDs are sometimes neutral, for example for mixed oxides with Pu. This could be used to distinguish between both type of defects with PAS in temperature since the trapping coefficient of negative vacancies decreases with temperature while it is constant for neutral defects[98]. In addition, since the dopant does not influence the lifetime, at least of the MOXs studied here, if PAS measurements on these systems find different lifetime values this will indicate that different type of defects are trapping the positron.

PAS measurements have been performed on UO_2[2, 4] and UO_2 with 0.2% plutonium weight content[3]. These studies found a short lifetime and long lifetime component around 170 and 310 ps that changes only slightly as a function of measurement temperature. The long lifetime component is thought to correspond to neutral and negative vacancies with similar PLT. When compared to our calculations this seems to indicate the presence of BSDs and uranium vacancies in the sample, as already mentioned in J. Wiktor *et al.*[4].

TABLE VII. Positron lifetimes calculated for fully relaxed neutral defects in $UPuAmO_2$ (25%Pu, 3%Am). The first number is for the neutral defect, the second one, if present, for the most stable charge state.

Defect	τ (ps)
-	162
V_O	165
V_O (Am)	165
V_U	300
V_U (Am)	299
BSD1	304
BSD2	312
BSD3	315

To go further, we performed calculations on a mixed oxide with U, Pu and Am. We add an Am atom on a $(U,Pu)O_2$ with a 25% Pu content. This corresponds to 3.125% of Am and 71.875% of U. The value of the volume for this compound is shown on Fig.5. It is aligned with the values of the $(U,Pu)O_2$ system. Concerning the valence charge states, the Am atom is III+ and one U atom becomes V+ to compensate. In terms of ionic radius, see table III, this combination is close to the replacement of one U^{IV+} by one Pu^{IV+}, in other words PuO_2 and AmO_2 have similar equilibrium volumes. We do not observe a new effect resulting of the presence of both Pu and Am in UO_2.

We also calculated the positron lifetime for this compound. It is similar to the values calculated without Am, see Table VII. We also test the position of the oxygen and uranium vacancy, with and without an Am in the first neighbors shell. The positron lifetime is not affected by the position of the vacancy.

IV. CONCLUSIONS

We performed a comparative study of 4 mixed oxides, UO_2 doped with La, Ce, Pu and Am. Concerning the lattice parameter's evolution with the doping content, we show that $(U,Am)O_2$ seems to deviate from the stoichiometric conditions in the experiments contrary to mixed oxides with La, Ce and Pu which follow the Vegard's law. We also show that the charge state of the point defects in mixed oxides are related to the valence of the doping element. For trivalent element the charge state of the defect is lower (negative) than if the doping element is tetravalent. This is related to the fact that with trivalent doping the charge transfer reaction U^{V+} to $^{IV+}$ (the valence state in UO_2) is favored with a negatively charge defect.

Our PLT calculations show that the doping element has almost no influence on the lifetime. We also hope that our these calculations will stimulate further experimental investigation like PAS to confirm that the same defects are present in different mixed oxides.

V. AKNOWLEDGEMENTS

This work was performed using high-performance computing resources from Grand Equipement National de Calcul Intensif (GENCI) [Centre Commun de Recherche et de Technologie (CCRT) and Centre Informatique National de l'Enseignement Supérieur (CINES)]. This research is part of the Investigations Supporting MOX Fuel Licensing in ESNII Prototype Reactors (INSPYRE).

[1] D. Prieur, L. Martel, J.-F. Vigier, A. C. Scheinost, K. O. Kvashnina, J. Somers, and P. M. Martin, Aliovalent Cation Substitution in UO_2 : Electronic and Local Structures of $U_{1-y}La_yO_{2\pm x}$ Solid Solutions, Inorganic Chemistry **57**, 1535 (2018), number: 3.

[2] M.-F. Barthe, H. Labrim, A. Gentils, P. Desgardin, C. Corbel, S. Esnouf, and J. P. Piron, Positron annihilation characteristics in UO2: for lattice and vacancy defects induced by electron irradiation, physica status solidi c **4**, 3627 (2007).

[3] D. Roudil, M. F. Barthe, C. Jégou, A. Gavazzi, and F. Vella, Investigation of defects in actinide-doped UO2 by positron annihilation spectroscopy, Journal of Nuclear Materials **420**, 63 (2012).

[4] J. Wiktor, M.-F. Barthe, G. Jomard, M. Torrent, M. Freyss, and M. Bertolus, Coupled experimental and DFT + U investigation of positron lifetimes in UO 2, Physical Review B **90**, 10.1103/PhysRevB.90.184101 (2014).

[5] S. L. Dudarev, D. N. Manh, and A. P. Sutton, Effect of Mott-Hubbard correlations on the electronic structure and structural stability of uranium dioxide, Philosophical Magazine B **75**, 613 (1997).

[6] M. Freyss, T. Petit, and J.-P. Crocombette, Point defects in uranium dioxide: Ab initio pseudopotential approach in the generalized gradient approximation, Journal of Nuclear Materials **347**, 44 (2005).

[7] B. Dorado, B. Amadon, M. Freyss, and M. Bertolus, $\text{DFT}+\text{U}$ calculations of the ground state and metastable states of uranium dioxide, Physical Review B **79**, 235125 (2009), number: 23 Publisher: American Physical Society.

[8] D. A. Andersson, B. P. Uberuaga, P. V. Nerikar, C. Unal, and C. R. Stanek, U and xe transport in $uo_{2\pm x}$: Density functional theory calculations, Phys. Rev. B **84**, 054105 (2011).

[9] J.-P. Crocombette, D. Torumba, and A. Chartier, Charge states of point defects in uranium oxide calculated with a local hybrid functional for correlated electrons, Physical Review B **83**, 184107 (2011).

[10] B. Dorado and P. Garcia, First-principles DFT+U modeling of actinide-based alloys: Application to paramagnetic phases of UO_2 and (U,Pu) mixed oxides, Physical Review B **87**, 195139 (2013).

[11] E. Vathonne, J. Wiktor, M. Freyss, G. Jomard, and M. Bertolus, DFT + U investigation of charged point defects and clusters in UO_2, Journal of Physics: Condensed Matter **26**, 325501 (2014), number: 32.

[12] F. Bruneval, M. Freyss, and J.-P. Crocombette, Lattice constant in nonstoichiometric uranium dioxide from first principles, Physical Review Materials **2**, 023801 (2018), number: 2.

[13] S. L. Dudarev, P. Liu, D. A. Andersson, C. R. Stanek, T. Ozaki, and C. Franchini, Parametrization of $\mathrm{LSDA}+U$ for noncollinear magnetic configurations: Multipolar magnetism in ${\mathrm{UO}}_{2}$, Physical Review Materials **3**, 083802 (2019), publisher: American Physical Society.

[14] L. Yang and B. D. Wirth, Clustering of excess oxygen in uranium dioxide: A first-principles study, Journal of Nuclear Materials , 153087 (2021).

[15] M. Payami, A DFT+U Study of the Ground State and Meta-Stable States of UO$_2$: The SMC Method, arXiv:2108.12758 [cond-mat] (2021).

[16] L. E. Ratcliff, L. Genovese, H. Park, P. B. Littlewood, and A. Lopez-Bezanilla, Exploring Metastable States in UO$_2$ using Hybrid Functionals and Dynamical Mean Field Theory, arXiv:2109.15084 [cond-mat] (2021).

[17] N.-D. Morelon, D. Ghaleb, J.-M. Delaye, and L. V. Brutzel, A new empirical potential for simulating the formation of defects and their mobility in uranium dioxide, Philosophical Magazine **83**, 1533 (2003).

[18] E. Yakub, C. Ronchi, and D. Staicu, Computer simulation of defects formation and equilibrium in nonstoichiometric uranium dioxide, Journal of Nuclear Materials **389**, 119 (2009).

[19] A. H. Tan, R. W. Grimes, and S. Owens, Structures of uo2 and puo2 surfaces with hydroxide coverage, Journal of Nuclear Materials **344**, 13 (2005), proceedings of the 11th International Symposium on Thermodynamics of Nuclear Materials.

[20] M. W. D. Cooper, M. J. D. Rushton, and R. W. Grimes, A many-body potential approach to modelling the thermomechanical properties of actinide oxides, Journal of Physics: Condensed Matter **26**, 105401 (2014), number: 10.

[21] M. W. D. Cooper, S. T. Murphy, and D. A. Andersson, The defect chemistry of UO2±x from atomistic simulations, Journal of Nuclear Materials **504**, 251 (2018).

[22] A. Soulié, F. Bruneval, M.-C. Marinica, S. Murphy, and J.-P. Crocombette, Influence of vibrational entropy on the concentrations of oxygen interstitial clusters and uranium vacancies in nonstoichiometric U O 2, Physical Review Materials **2** (2018), number: 8.

[23] S. C. Middleburgh, W. E. Lee, and M. J. D. Rushton, Structure and properties of amorphous uranium dioxide, Acta Materialia **202**, 366 (2021).

[24] D. Bathellier, M. Lainet, M. Freyss, P. Olsson, and E. Bourasseau, A new heat capacity law for UO2, PuO2 and (U,Pu)O2 derived from molecular dynamics simulations and useable in fuel performance codes, Journal of Nuclear Materials **549**, 152877 (2021).

[25] G. Jomard, B. Amadon, F. Bottin, and M. Torrent, Structural, thermodynamic, and electronic properties of plutonium oxides from first principles, Physical Review B **78**, 075125 (2008), number: 7 Publisher: American Physical Society.

[26] L. Shi, E. Vathonne, V. Oison, M. Freyss, and R. Hayn, First-principles DFT+U investigation of charged states of defects and fission gas atoms in ${\mathrm{CeO}}_{2}$, Physical Review B **94**, 115132 (2016).

[27] M. S. Talla Noutack, G. Geneste, G. Jomard, and M. Freyss, First-principles investigation of the bulk properties of americium dioxide and sesquioxides, Physical Review Materials **3**, 035001 (2019), number: 3 Publisher: American Physical Society.

[28] B. Li and H. Metiu, Dft studies of oxygen vacancies on undoped and doped la2o3 surfaces, The Journal of Physical Chemistry C **114**, 12234 (2010).

[29] I. C. Njifon, M. Bertolus, R. Hayn, and M. Freyss, Electronic Structure Investigation of the Bulk Properties of Uranium–Plutonium Mixed Oxides (U, Pu)O2, Inorganic Chemistry **57**, 10974 (2018), publisher: American Chemical Society.

[30] M. S. T. Noutack, G. Jomard, M. Freyss, and G. Geneste, Journal of Physics: Condensed Matter **31**, 485501 (2019), publisher: IOP Publishing.

[31] B. E. Hanken, C. R. Stanek, N. Grønbech-Jensen, and M. Asta, Computational study of the energetics of charge and cation mixing in $u_{1-x}ce_xo_2$, Phys. Rev. B **84**, 085131 (2011).

[32] J. Solomon, V. Alexandrov, B. Sadigh, A. Navrotsky, and M. Asta, Computational study of the energetics and defect clustering tendencies for y- and la-doped uo2, Acta Materialia **78**, 282 (2014).

[33] The ABINIT code is a common project of the Catholic University of Louvain (Belgium), Corning Incorporated, CEA (France) and other collaborators (URL http://www.abinit.org).

[34] X. Gonze, B. Amadon, G. Antonius, F. Arnardi, L. Baguet, J.-M. Beuken, J. Bieder, F. Bottin, J. Bouchet, E. Bousquet, N. Brouwer, F. Bruneval, G. Brunin, T. Cavignac, J.-B. Charraud, W. Chen, M. Côté, S. Cottenier, J. Denier, G. Geneste, P. Ghosez, M. Giantomassi, Y. Gillet, O. Gingras, D. R. Hamann, G. Hautier, X. He, N. Helbig, N. Holzwarth, Y. Jia, F. Jollet, W. Lafargue-Dit-Hauret, K. Lejaeghere, M. A. Marques, A. Martin, C. Martins, H. P. Miranda, F. Naccarato, K. Persson, G. Petretto, V. Planes, Y. Pouillon, S. Prokhorenko, F. Ricci, G.-M. Rignanese, A. H. Romero, M. M. Schmitt, M. Torrent, M. J. van Setten, B. V. Troeye, M. J. Verstraete, G. Zérah, and J. W. Zwanziger, The abinitproject: Impact, environment and recent developments, Computer Physics Communications **248**, 107042 (2020).

[35] A. H. Romero, D. C. Allan, B. Amadon, G. Antonius, T. Applencourt, L. Baguet, J. Bieder, F. Bottin, J. Bouchet, E. Bousquet, F. Bruneval, G. Brunin, D. Caliste, M. Côté, J. Denier, C. Dreyer, P. Ghosez, M. Giantomassi, Y. Gillet, O. Gingras, D. R. Hamann, G. Hautier, F. Jollet, G. Jomard, A. Martin, H. P. C. Miranda, F. Naccarato, G. Petretto, N. A. Pike, V. Planes, S. Prokhorenko, T. Rangel, F. Ricci, G.-M. Rignanese, M. Royo, M. Stengel, M. Torrent, M. J. van Setten, B. Van Troeye, M. J. Verstraete, J. Wiktor, J. W. Zwanziger, and X. Gonze, ABINIT: Overview and focus on selected capabilities, The Journal of Chemical Physics **152**, 124102 (2020), number: 12 _eprint: https://doi.org/10.1063/1.5144261.

[36] P. E. Blöchl, Projector augmented wave method, Phys. Rev. B **50**, 17953 (1994).

[37] M. Torrent, F. Jollet, F. Bottin, G. Zerah, and X. Gonze, Implementation of the projector augmented-wave method in the abinit code: Application to the study of iron under pressure, Comput. Mater. Sci. **42**, 337 (2008).

[38] J. P. Perdew, K. Burke, and M. Ernzerhof, Phys. Rev. Lett. **77**, 3865 (1996).

[39] M. H. J and P. J. D, Special points for brillouin zone integrations, Physical Review B **13**, 5188 (1976).

[40] A. I. Liechtenstein, V. I. Anisimov, and J. Zaanen, Density-functional theory and strong interactions: Orbital ordering in Mott-Hubbard insulators, Physical Review B **52**, R5467 (1995), publisher: American Physical Society.

[41] B. Dorado, G. Jomard, M. Freyss, and M. Bertolus, Stability of oxygen point defects in UO_2 by first-principles DFT + U calculations: Occupation matrix control and Jahn-Teller distortion, Physical Review B **82**, 035114 (2010).

[42] R. M. Nieminen, E. Boronski, and L. J. Lantto, Two-component density-functional theory: Application to positron states, Physical Review B **32**, 1377 (1985), number: 2 Publisher: American Physical Society.

[43] E. Boroński and R. M. Nieminen, Electron-positron density-functional theory, Physical Review B **34**, 3820 (1986), number: 6 Publisher: American Physical Society.

[44] M. J. Puska, A. P. Seitsonen, and R. M. Nieminen, Electron-positron Car-Parrinello methods: Self-consistent treatment of charge densities and ionic relaxations, Physical Review B **52**, 10947 (1995), publisher: American Physical Society.

[45] J. Wiktor, G. Jomard, and M. Torrent, Two-component density functional theory within the projector augmented-wave approach: Accurate and self-consistent computations of positron lifetimes and momentum distributions, Physical Review B **92**, 125113 (2015), number: 12 Publisher: American Physical Society.

[46] A. Zunger, S.-H. Wei, L. G. Ferreira, and J. E. Bernard, Special quasirandom structures, Physical Review Letters **65**, 353 (1990), number: 3 Publisher: American Physical Society.

[47] J.-P. Crocombette, enInfluence of charge states on energies of point defects and clusters in uranium dioxide, Physical Review B **85**, 144101 (2012).

[48] S. E. Taylor and F. Bruneval, Understanding and correcting the spurious interactions in charged supercells, Physical Review B **84**, 075155 (2011), number: 7.

[49] S. Lany and A. Zunger, Accurate prediction of defect properties in density functional supercell calculations, Modelling and Simulation in Materials Science and Engineering **17**, 084002 (2009), number: 8.

[50] M. Leslie and N. J. Gillan, The energy and elastic dipole tensor of defects in ionic crystals calculated by the supercell method, Journal of Physics C: Solid State Physics **18**, 973 (1985), number: 5.

[51] S. Na-Phattalung, M. F. Smith, K. Kim, M.-H. Du, S.-H. Wei, S. B. Zhang, and S. Limpijumnong, First-principles study of native defects in anatase ${\mathrm{Ti}}{\mathrm{O}}_{2}$, Physical Review B **73**, 125205 (2006), number: 12 Publisher: American Physical Society.

[52] M. Hong, S. R. Phillpot, C.-W. Lee, P. Nerikar, B. P. Uberuaga, C. R. Stanek, and S. B. Sinnott, Solubility and clustering of ruthenium fission products in uranium dioxide as determined by density functional theory, Physical Review B **85**, 144110 (2012), number: 14 Publisher: American Physical Society.

[53] R. J. M. Konings, O. Beneš, A. Kovács, D. Manara, D. Sedmidubský, L. Gorokhov, V. S. Iorish, V. Yungman, E. Shenyavskaya, and E. Osina, The Thermodynamic Properties of the f-Elements and their Compounds. Part 2. The Lanthanide and Actinide Oxides, Journal of Physical and Chemical Reference Data **43**, 013101 (2014), publisher: American Institute of Physics.

[54] P. Martin, S. Grandjean, C. Valot, G. Carlot, M. Ripert, P. Blanc, and C. Hennig, XAS study of $(U_{1-y}Pu_y)O_2$ solid solutions, Journal of Alloys and Compounds Proceedings of the Plutonium Futures - The Science 2006 Conference, **444-445**, 410 (2007).

[55] J. Schoenes, Optical properties and electronic structure of UO2, Journal of Applied Physics **49**, 1463 (1978), publisher: American Institute of Physics.

[56] A. Debernardi and A. Debernardi, Ab initio calculation of band alignment of epitaxial La_2O_3 on Si(111) substrate, AIMS Materials Science **2**, 279 (2015), cc_license_type: cc_by Primary_atype: AIMS Materials Science Subject_term: Research article Subject_term_id: Research article.

[57] R. Venkata Krishnan, G. Panneerselvam, M. P. Antony, and K. Nagarajan, Solubility studies and thermal expansion coefficient of uranium–lanthanum mixed oxide system, Journal of Nuclear Materials **403**, 25 (2010), number: 1.

[58] S. Ohmi, C. Kobayashi, I. Kashiwagi, C. Ohshima, H. Ishiwara, and H. Iwai, Characterization of La2 O 3 and Yb2 O 3 Thin Films for High-k Gate Insulator Application, Journal of The Electrochemical Society **150**, F134 (2003), publisher: IOP Publishing.

[59] L. Gerward, J. Staun Olsen, L. Petit, G. Vaitheeswaran, V. Kanchana, and A. Svane, Bulk modulus of CeO2 and PrO2—An experimental and theoretical study, Journal of Alloys and Compounds **400**, 56 (2005).

[60] D. R. Mullins, S. H. Overbury, and D. R. Huntley, Electron spectroscopy of single crystal and polycrystalline cerium oxide surfaces, Surface Science **409**, 307 (1998).

[61] E. Wuilloud, B. Delley, W. D. Schneider, and Y. Baer, Spectroscopic Evidence for Localized and Extended f-Symmetry States in Ce${\mathrm{O}}_{2}$, Physical Review Letters **53**, 202 (1984), publisher: American Physical Society.

[62] C. E. McNeilly, The electrical properties of plutonium oxides, Journal of Nuclear Materials **11**, 53 (1964).

[63] C. Suzuki, T. Nishi, M. Nakada, M. Akabori, M. Hirata, and Y. Kaji, Core-hole effect on XANES and electronic structure of minor actinide dioxides with fluorite structure, Journal of Physics and Chemistry of Solids **73**, 209 (2012).

[64] C. Hurtgen and J. Fuger, Self-irradiation effects in americium oxides, Inorganic and Nuclear Chemistry Letters **13**, 179 (1977).

[65] J. Wang, R. C. Ewing, and U. Becker, Electronic structure and stability of hyperstoichiometric uo_{2+x} under pressure, Phys. Rev. B **88**, 024109 (2013).

[66] L. Vegard, Die konstitution der mischkristalle und die raumfullung der atome, Eur. Phys. J. A **5**, 17 (1921).

[67] D. Parfitt, K. H. Desai, and R. W. Grimes, *Atomic-scale simulation of soluble fission products in UO2* (Publications Office of the European Union, 2009).

[68] Z. Talip, T. Wiss, P. E. Raison, J. Paillier, D. Manara, J. Somers, and R. J. M. Konings, Raman and X-ray Studies of Uranium–Lanthanum-Mixed Oxides Before and After Air Oxidation, Journal of the American Ceramic Society **98**, 2278 (2015), number: 7.

[69] D. C. Hill, Phase Relations and Crystal Chemistry in the System Uranium Oxide–Lanthanum Oxide, Journal of the American Ceramic Society **45**, 258 (1962), number: 6.

[70] E. Stadlbauer, U. Wichmann, U. Lott, and C. Keller, Thermodynamics and phase relationships of the ternary lanthanum-uranium-oxygen system, Journal of Solid State Chemistry **10**, 341 (1974), number: 4.

[71] P. Herrero, R. M. Rojas, and P. García, The UCaLaO and ULaO systems: a comparative study, Inorganica Chimica Acta **140**, 159 (1987).

[72] T. Tsuji, M. Iwashita, T. Yamashita, and K. Ohuchi, Effect of cations on lattice constants of $(m_yu_{1y}o_2$ (m=pu, th, la) at low doped cation concentrations, Journal of Alloys and Compounds **271-273**, 391 (1998).

[73] W. B. Wilson, C. A. Alexander, and A. F. Gerds, Stabilization of UO2, Journal of Inorganic and Nuclear Chemistry **20**, 242 (1961), number: 3.

[74] F. Hund, R. Wagner, and U. Peetz, Anomalous mixed crystals in the system cerium dioxide-uranium dioxide, Zeitschrift for Elektrochem **56**, 61 (1952).

[75] S. M. Lang, F. P. Knudsen, C. L. Fillmore, and R. S. Roth, *High-temperature reactions of uranium dioxide with various metal oxides.*, Tech. Rep. (Technical Report NBS-C-568, National Bureau of Standards, Washington, D.C., 1956).

[76] A. Magneli and L. Kihlborg, On the cerium dioxide-uranium dioxide system and "uranium cerium blue", Acta Chemica Scandinavica **5**, 578 (1951).

[77] T. L. Markin, R. S. Street, and E. C. Crouch, The uranium-cerium-oxygen ternary phase diagram, Journal of Inorganic and Nuclear Chemistry **32**, 59 (1970).

[78] W. Rudorff and G. Valet, Uber das ceruranblau und mischkristalle im system ceo2-uo2-u3o8, Zeitschrift fur anorganische und allgemeine Chemie **271**, 257 (1953).

[79] K. Yamada, S. Yamanaka, and M. Katsura, Physicochemical properties of (U,Ce)O2, Journal of Alloys and Compounds **275-277**, 725 (1998).

[80] E. J. McIver, *Unit cell size of solid solutions of uranium dioxide and fission product oxides*, Tech. Rep. (Technical Report AERE-M-1612, Atomic Energy Research Establishment, Harwell England, 1966).

[81] H. Cao, H. Bao, X. Lin, J. Lin, L. Zhang, Y. Huang, and J.-Q. Wang, Differential interplay between Ce and U on local structures of $u_{1-x}ce_xo_2$ solid solutions probed by X-ray absorption spectroscopy, Journal of Nuclear Materials **515**, 238 (2019).

[82] D. I. R. Norris and P. Kay, Oxygen potential and lattice parameter measurements in (U, Ce)O2 zx, Journal of Nuclear Materials **116**, 184 (1983).

[83] M. Kato and K. Konashi, Lattice parameters of (U, Pu, Am, Np)O2x, Journal of Nuclear Materials Plutonium Futures - The Science 2008, **385**, 117 (2009).

[84] C. Takoukam-Takoundjou, E. Bourasseau, M. J. D. Rushton, and V. Lachet, Optimization of a new interatomic potential to investigate the thermodynamic prop-

erties of hypo-stoichiometric mixed oxide fuel U1-y Pu y O2-x, **32**, 505702 (2020), publisher: IOP Publishing.

[85] T. Ohmichi, S. Fukushima, A. Maeda, and H. Watanabe, On the relation between lattice parameter and o/m ratio for uranium dioxide-trivalent rare earth oxide solid solution, Journal of Nuclear Materials **102**, 40 (1981).

[86] C. Duriez, J.-P. Alessandri, T. Gervais, and Y. Philipponneau, Thermal conductivity of hypostoichiometric low pu content (u,pu)o2x mixed oxide, Journal of Nuclear Materials **277**, 143 (2000).

[87] D. Prieur, P. M. Martin, A. Jankowiak, E. Gavilan, A. C. Scheinost, N. Herlet, P. Dehaudt, and P. Blanchart, Local structure and charge distribution in mixed uranium–americium oxides: Effects of oxygen potential and am content, Inorganic Chemistry **50**, 12437 (2011).

[88] D. Prieur, F. Lebreton, M. Caisso, P. M. Martin, A. C. Scheinost, T. Delahaye, and D. Manara, Melting behaviour of americium-doped uranium dioxide, The Journal of Chemical Thermodynamics **97**, 244 (2016).

[89] K. Mayer, B. Kanellakopoulos, J. Naegele, and L. Koch, On the valency state of americium in $(U_{0.5}Am_{0.5})O_{2-x}$, Journal of Alloys and Compounds International Conference on Actinides, **213-214**, 456 (1994).

[90] F. Lebreton, D. Horlait, T. Delahaye, and P. Blanchart, Fabrication and characterization of $(U_{1-x}Am_x)O_{2\pm\delta}$ compounds with high americium contents (x=0.3, 0.4 and 0.5), Journal of Nuclear Materials **439**, 99 (2013).

[91] M. Vespa, M. Rini, J. Spino, T. Vitova, and J. Somers, Fabrication and characterization of (U, Am)O2x transmutation targets, Journal of Nuclear Materials **421**, 80 (2012).

[92] F. Lebreton, D. Horlait, R. Caraballo, P. M. Martin, A. C. Scheinost, A. Rossberg, C. Jégou, and T. Delahaye, Peculiar Behavior of $(U,Am)O_{2-\delta}$ Compounds for High Americium Contents Evidenced by XRD, XAS, and Raman Spectroscopy, Inorganic Chemistry **54**, 9749 (2015).

[93] J. Bouchet and F. Bottin, Thermal evolution of vibrational properties of -U, Physical Review B - Condensed Matter and Materials Physics **92** (2015), number: 17.

[94] J. Bouchet and F. Bottin, High-temperature and high-pressure phase transitions in uranium, Physical Review B **95**, 054113 (2017), publisher: American Physical Society.

[95] B. Dorado, F. Bottin, and J. Bouchet, Phonon spectra of plutonium at high temperatures, Physical Review B **95** (2017), number: 10.

[96] A. Kokalj, J. Mol. Graph. Model. **17**, 176 (1999).

[97] A. Kokalj, Comput. Mat. Sci. **28**, 155 (2003).

[98] M. J. Puska and R. M. Nieminen, Theory of positrons in solids and on solid surfaces, Reviews of Modern Physics **66**, 841 (1994), number: 3 Publisher: American Physical Society.